ACS SyntheticBiology

pubs.acs.org/synthbio Research Article

Carbon Metabolism Modification in *Bacillus subtilis* for Improving Fengycin Production and Investigating Antifungal Activity of Its Homologous Components

Dun-Ju Wang,[⊥] Ming-Zhu Ding,[⊥] Zheng-Jie Hou, Yong Zhang, Wei Shang, Tian-Xu Duan, Qiu-Man Xu,* and Jing-Sheng Cheng*

Cite This: *ACS Synth. Biol.* 2025, 14, 2644−2656 Read Online

ACCESS | Metrics & More | Article Recommendations | Supporting Information

ABSTRACT: As a lipopeptide, fengycin exhibits environmentally friendly, safe, and long-lasting biocontrol efficacy. However, due to its complex structure and the challenges in chemical synthesis, it is primarily produced through biosynthesis. This study reports an improvement in fengycin production in *Bacillus subtilis* by engineering the central carbon metabolic pathway and blocking the carbon overflow pathway. The highest production achieved 1290.31 mg/L, representing a 2.05-fold increase compared to the original strain. Additionally, a coculture system was established in which *Corynebacterium glutamicum* supplied proline to strain CGF-PA, achieving a further increase in production to 2491.97 mg/L. The fengycin homologues were characterized using IMS-MS and separated by preparative liquid chromatography. The antifungal activities of fengycin homologues were quantitatively evaluated against *Fusarium graminearum*, *Botrytis cinerea*, *Pyricularia oryzae*, and *Rhizoctonia solani*, and their morphological changes were observed. The study also investigated the differences in antifungal activity among the fengycin variants. Components 4, 5, 6, and 7 exhibited relatively strong antifungal activity, and the various components of fengycin were found to work synergistically.

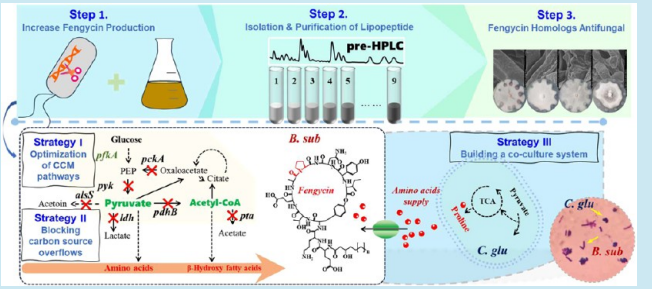

KEYWORDS: *fengycin homologues, carbon pathway modification, byproducts, coculture, antifungal activity*

1. INTRODUCTION

Fengycin is a lipopeptide produced by nonribosomal peptide synthetase (NRPS),[1] which has significant antifungal,[2] antitumor,[3] and antiviral activities.[4] As a biosurfactant, it offers distinct advantages over chemical surfactants due to its low toxicity, biodegradability, biocompatibility, ease of production from renewable resources, and high selectivity and stability under extreme conditions of temperature, pH, and salinity.[5] Recent approaches include fermentation optimization and metabolic engineering, which utilize enhanced precursor supply, regulatory factors, promoter engineering, and genome engineering.[6] The highest single-strain fengycin production stands at 1400 mg/L in medium with exogenously added fatty acids and amino acids.[7] In contrast, single-strain fengycin production typically remains below 1000 mg/L under HPLC detection. Cellular metabolism encompasses thousands of reactions that involve the biosynthesis of cell components through limited precursor metabolites, such as glucose 6-phosphate, fructose-6-phosphate, and ribose 5-phosphate, formed in primary metabolism and contributing to the degradation process. Therefore, it is significant to optimize biomass and fengycin production by restructuring these central carbon metabolic pathways.[8] In most bacteria, the main pathways of central metabolism are the Embden−Meyerhof−Parnas pathway or the Entner−Doudoroff pathway and the tricarboxylic acid (TCA) cycle, with the interconversion of metabolites at the phosphoenolpyruvate-pyruvate-oxaloacetate node involving a set of structurally entangled reactions that interconnect these carbon metabolism pathways, responsible for the distribution of carbon flux between catabolism, anabolism, and cellular energy supply, while also forming an ATP dissipation futile cycle.[9] Research has shown that dynamically downregulating the expression of pyruvate kinase to control pyruvate formation and redistribute metabolic flux between cell growth and the biosynthesis of 2-pyrone-4,6-dicarboxylic acid significantly improved its production.[10] In a glucose-containing medium, *Bacillus subtilis* acts as a mixed acid fermenter, converting pyruvate into lactic acid, acetate, ethanol, acetoin, and 2,3-butanediol as final fermentation products.[11] An inverse

Received: February 10, 2025
Revised: June 8, 2025
Accepted: June 9, 2025
Published: June 17, 2025

https://doi.org/10.1021/acssynbio.5c00101
ACS Synth. Biol. 2025, 14, 2644−2656

relationship has been found between the carbon flux of lipopeptides and primary metabolism.[12] Further studies should be conducted to direct the carbon flux toward lipopeptide production.

The structure of fengycin can be generally described as comprising 10 α-amino acids and a β-hydroxy fatty acid with a side chain length of 14−21 carbon atoms.[13] Due to its specific amino acid structure, fengycin exhibits distinct behavior in mass spectrometry, with the precursor ion primarily fragmenting at the Glu-Orn and Orn-Tyr bonds to generate specific octapeptide ring ions[14] (Table S1). These fragments serve as distinct "fingerprints" of various fengycin homologues, indicating differences in the amino acid composition of the peptide chain with minimal relation to fatty acid tails, thereby facilitating rapid analysis and inference of fatty acid chain length in fengycin homologues.[15] The specific composition and proportions of amino acids can be determined through acid hydrolysis and the phenyl isothiocyanate derivatization method.[14]

Co-cultivation engineering has emerged as a promising strategy for heterologous biosynthesis, offering significant improvements in target product production.[16] This approach facilitates the exchange and interaction of small molecules produced between cells, alleviates metabolic burdens through division of labor, and stabilizes the system through flexible metabolic module distribution and microbial ratio regulation. These factors improve substrate utilization and target product yield. After optimizing the inoculation time and ratio, the coculture system of *Corynebacterium glutamicum* cgb-11 and *B. subtilis* CGF26-IV achieved a 2.9-fold increase in fengycin production compared to monoculture, with fengycin production reaching 1760 mg/L.[7]

Antifungal activity is an important application of fengycin. Fengycin exhibits inhibitory effects against various fungal species, including *Fusarium graminearum*,[17] *Rhizoctonia solani*,[18] *Pyricularia oryzae*,[19] and *Botrytis cinerea*.[20] It was demonstrated that fengycin affects biological membranes differently depending on the molar ratios.[21] The extent of fengycin's effect on membrane leakage is determined by a balance between hydrophobic interactions among Tyr-10, Tyr-4, and Ile-11, and favorable electrostatic interactions between the charged residues (Glu and Orn) and the lipid head groups.[22] However, the effectiveness of fengycin may vary as more variants are discovered.

To enhance fengycin biosynthesis, gene modification has been successfully conducted to regulate central carbon metabolism and remove byproducts generated during central metabolism, thereby constructing high-yield *B. subtilis*. These modified high-yield *B. subtilis* strains will then be cocultured with *C. glutamicum* to further enhance fengycin production. The components obtained from the separation and purification of fengycin will be used for further antifungal experiments. This study provides feasible genetic engineering methods to enhance fengycin production and offers reliable references for further exploration of fengycin's antifungal mechanisms.

2. MATERIALS AND METHODS

2.1. Strains and Plasmids. All strains and plasmids used in this study are listed in Table S2. *Escherichia coli* DH5α was used for plasmid construction and transformation. The pJOE8999 plasmid was cloned in *E. coli* DH5α strain and subsequently delivered into *B. subtilis*. Fengycin is produced by the laboratory-stored recombinant strain *B. subtilis* CGF-PG and its derivatives. Proline was generated by the laboratory-stored recombinant strain *C. glu-proline*. *Fusarium graminearum*, *Botrytis cinerea*, *Pyricularia oryzae*, and *Rhizoctonia solani* were used as indicator fungi in the antifungal experiments.

2.2. Plasmids and Strains Construction. *2.2.1. Plasmids Construction.* The pJOE8999-derived plasmid was constructed using a seamless cloning one-step assembly method. The construction method for the sgRNA-containing pJOE-sgRNA was adapted from a previous study.[23] The linearized plasmid s-pJOE-sgRNA was obtained by cleaving the pJOE-sgRNA plasmid using *Sfi* I restriction endonuclease (New England Biolabs, Beijing, China). The upstream and downstream homologous arms, promoter, target gene, and s-pJOE-sgRNA were then assembled using a seamless cloning kit (Vazyme, Nanjing, China) to obtain the final target plasmid. All primer sequences used in this study are listed in Table S3.

2.2.2. Construction of Recombinant Strains. Competent cells of *B. subtilis* CGF-PG and its derivatives were prepared using the Spizizen chemical transformation method, and the recombinant plasmids were subsequently introduced into these cells.[23] The appropriate strains were streaked on Luria−Bertani (LB) agar plates (10 g/L tryptone, 5 g/L yeast extract, 10 g/L NaCl, and 20 g/L agar). Strains were incubated at 50 °C to promote plasmid loss, then streaked on LB plates with and without kanamycin to verify plasmid curing.

2.3. Shake Flask Cultivation. In the pure culture and coculture processes, the primary seed medium for *B. subtilis* was LB liquid medium, while the primary seed medium for *C. glutamicum* was BHI medium (37.0 g/L). The secondary seed medium and the fermentation medium were identical. Fermentation medium included:[24] Cal18 medium (50.0 g/L maltodextrin, 40.0 g/L yeast extract, 1.3 g/L $MgSO_4{\cdot}7H_2O$, 20.0 g/L $Na_2HPO_4{\cdot}12H_2O$, and 6.7 g/L $Na_2MoO_4{\cdot}2H_2O$, pH 7.0); Cal18−7 medium (40.0 g/L maltodextrin, 10.0 g/L sucrose, 10.0 g/L yeast extract, 1.3 g/L $MgSO_4{\cdot}7H_2O$, 20.0 g/L $Na_2HPO_4{\cdot}12H_2O$, 6.7 g/L $Na_2MoO_4{\cdot}2H_2O$, 3.0 g/L KH_2PO_4, 5.0 g/L $(NH_4)_2SO_4$, 0.02 g/L $FeSO_4$, 0.02 g/L $MnSO_4$, 0.45 mg/L vitamin B_1, and 0.05 mg/L vitamin B_7). To prepare the seed cultures of *B. subtilis*, single colonies from LB plates were inoculated into 5.0 mL of LB medium and incubated at 37 °C with shaking at 200 rpm for 24 h. Subsequently, the seed culture was transferred to 80 mL of fermentation medium at an initial OD_{600} of 0.2 and incubated at 30 °C with shaking at 180 rpm for 12 h. After 12 h, the culture was incubated for an additional 72 h under the same conditions. Fengycin production was analyzed after 72 h of fermentation.

In the coculture fermentation, the seed culture of *B. subtilis* was consistent with the pure culture. To prepare the seed cultures of *C. glutamicum*, single colonies on BHI plates were inoculated into 5.0 mL of BHI medium and incubated at 30 °C with shaking at 200 rpm for 12 h. Subsequently, the seed culture was transferred to the secondary seed medium at an initial OD_{600} of 0.2 and incubated for 24 h at 30 °C with shaking at 180 rpm. Finally, the seed culture was inoculated into the fermentation medium.

2.4. Extraction and Identification of Fengycin. *2.4.1. Extraction of Fengycin.* The extraction of fengycin was performed as previously described.[25] The fermentation broth was centrifuged, and the supernatant was acidified to pH 2 with 6 mol/L HCl. The acidified solution was then stored at 4 °C for 12 h. The resulting precipitate was collected by centrifugation, lyophilized, and extracted with methanol. Methanol was removed using a rotary evaporator, and fengycin was dissolved

https://doi.org/10.1021/acssynbio.5c00101
ACS Synth. Biol. 2025, 14, 2644−2656

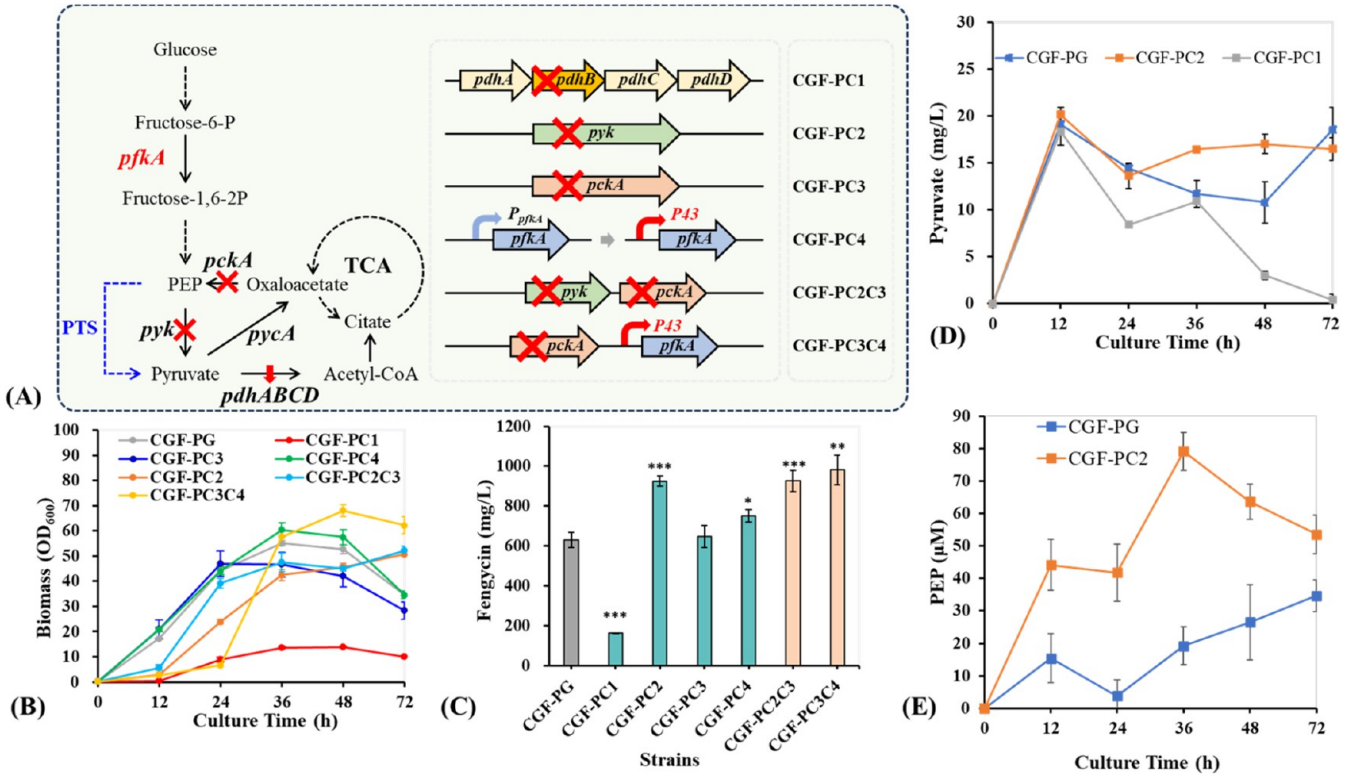

Figure 1. Effect of central carbon metabolism modification on fengycin production in *B. subtilis*. (A) Schematic diagram of central carbon metabolism. Red text indicates overexpression; red crosses (×) represent knockout. (B) Biomass (OD_{600}) of recombinant *B. subtilis*. (C) Fengycin production by recombinant *B. subtilis*. (D) Pyruvate content. (E) PEP content. * $p < 0.05$, ** $p < 0.01$, *** $p < 0.001$.

in chromatographic-grade methanol for analysis by high-performance liquid chromatography (HPLC).

2.4.2. Identification of Fengycin. Fengycin in the crude extract was analyzed by HPLC on a C18 column (4.6 × 150 mm, 5 μm; Agilent Technologies, Santa Clara, CA, USA). The mobile phase consisted of 50% acetonitrile and 50% purified water containing 0.1% (v/v) trifluoroacetic acid (TFA). Detection was performed at a wavelength of 210 nm. The column temperature was maintained at 30 °C, the flow rate was 0.8 mL/min, and the injection volume was 10.0 μL.[26]

2.4.3. Preparation of Liquid-Phase Separation and Purification of Fengycin. Fengycin in the crude extract was separated by preparative HPLC on a C18 reversed-phase column (10 × 150 mm, 5 μm; Welch Materials, Shanghai, China). The mobile phase consisted of 48% acetonitrile and 52% purified water containing 0.1% (v/v) TFA. The column temperature was maintained at ambient conditions, the flow rate was 4.7 mL/min, and the injection volume was adjusted based on the sample concentration. Elution of fengycin was monitored by UV detection at 210 nm. Fractions corresponding to individual peaks were collected in separate vials, concentrated under reduced pressure, lyophilized, and subjected to further mass spectrometric characterization.

The fengycin component samples were then analyzed by Ion Mobility High-Resolution Liquid Mass Spectrometer (Waters SELECT SERIES Cyclic IMS, American) equipped with an electrospray ionization source. Data acquisition was performed in positive ion mode with full scan detection over a mass range of m/z 50−2000.

2.5. Detection of Metabolic Intermediates and By-products. *2.5.1. Acetoin and Acetic Acid Determination.* The fermentation broth was centrifuged, and the supernatant was collected. Standard solutions of different concentrations were prepared using acetoin and acetic acid standards. Both the supernatant and the standard solutions were filtered through a 0.45 μm microporous membrane. The acetoin and acetic acid contents were determined by HPLC.[27] The analysis was performed using an Agilent Aminex HPX-87H Ion Exclusion column (7.8 mm × 300 mm, 5 μm) coupled with a refractive index detector. The mobile phase was 5 mmol/L sulfuric acid, the column temperature was set at 65 °C, the injection volume was 10 μL, and the flow rate was 0.6 mL/min.

2.5.2. Phosphoenolpyruvate (PEP) Determination. The PEP content was detected using the Amplex Red phosphoenolpyruvate assay kit (Beyotime, Shanghai, China). *B. subtilis* was washed with PBS and then collected by centrifugation. The bacteria were lysed using ultrasonication, and the supernatant was collected for analysis after centrifugation. In a 96-well plate, 2 μL of the standard/sample was added, followed by 80 μL of the Amplex Red reaction working solution. The mixture was thoroughly mixed and incubated at 37 °C in the dark for 30 min. Fluorescence detection was performed using an excitation wavelength of 560 nm and an emission wavelength of 590 nm to measure the fluorescence intensity.

2.5.3. Pyruvate Determination. Pyruvate detection was performed using the pyruvate assay kit (Biotopped, Beijing, China). *B. subtilis* was washed with PBS and then collected by centrifugation. The bacteria were lysed using ultrasonication, and the supernatant was collected for analysis after centrifugation. In a 96-well plate, 75 μL of the sample/pyruvate standard solution/distilled water was added, followed by 25 μL of the phenylhydrazine color reagent, and mixed thoroughly. Finally, 125 μL of the PA Assay Buffer was added, mixed, and allowed to

https://doi.org/10.1021/acssynbio.5c00101
ACS Synth. Biol. 2025, 14, 2644−2656

stand. The absorbance was measured at 520 nm. Calculate the pyruvate content based on the standard curve.

2.5.4. Proline Determination. After derivatization of proline with PITC (phenyl isothiocyanate), quantitative determination was performed using HPLC. The chromatographic column used was Venusil AA (4.6 × 250 mm, 5 μm) (Agela Technologies, Tianjin, CA, China). The mobile phase and the determination conditions were the same as those in the previous report.[7]

2.6. Antifungal Activity Assay. To quantify the inhibitory effect of fengycin on various fungi, mycelial agar plugs (0.8 cm in diameter) from four fungal species were inoculated onto PDA plates supplemented with 50 mg/L fengycin product (treatment group) and control PDA plates (CT). The colony diameters and morphological characteristics were recorded daily. Colony growth diameters were measured using the cross method (averaging two perpendicular diameters).

The antifungal activity of fengycin homologues was assayed using the Oxford cup method.[7] Methanol was used to extract the fengycin from the crude product and purified fengycin from liquid chromatography was diluted to 50 mg/L. Mycelial agar plugs from fungal cultures were placed at the center of PDA plates. After incubation at 30 °C for 24−36 h, 200 μL fengycin extract was added to each Oxford cup. The PDA plates inoculated with indicator strains were then incubated at 30 °C for 48−72 h to evaluate the antifungal activity of fengycin.[23]

2.7. Scanning Electron Microscopy (SEM). Fungal cultures were grown on PDA plates containing 50 mg/L fengycin and on control PDA plates. Mycelia were harvested and prepared for scanning electron microscopy (SEM) analysis. An appropriate amount of mycelium was placed on carbon-conductive adhesive tape and sputter-coated with a gold layer using a gold coater. The specimens were observed under a scanning electron microscope (HITACHI Regulus 8100, Hitachi High-Tech Corporation, Tokyo, Japan). Two scans were acquired at different magnifications for each treatment. Scale bars indicating specific lengths are provided in each image.

2.8. Statistical Analyses. All the above experiments were repeated three times. Significant differences were indicated at $p < 0.05$ (*), highly significant differences were indicated at $p < 0.01$ (**), and very highly significant differences were indicated at $p < 0.001$ (***).

3. RESULTS AND DISCUSSION

3.1. Impact of Carbon Source Pathway Modification. The genetic modification performed in this chapter are shown in Figure 1A. The *B. subtilis* CGF-PG strain exhibited robust growth capability (Figure 1B). To minimize resource waste during the growth process and enhance the cost-effectiveness of fengycin production, specific genes in the central carbon metabolism pathway were knocked out (Figure 1A). The *pdhABCD* operon of *B. subtilis* encodes the components of the pyruvate dehydrogenase (PDH) complex, including E1α and E1β (pyruvate decarboxylase), E2 (dihydrolipoamide acetyltransferase), and E3 (dihydrolipoamide dehydrogenase). The knockout of *pdhB* significantly reduced the growth of the strain (Figure 1B). The knockout of the *pdhB* gene resulted in a 74% reduction in fengycin production by strain CGF-PC1 (Figure 1C). The observed growth inhibition is likely due to loss of PDH activity resulting in acetyl-CoA deficiency (not detected) and reduced pyruvate content (Figure 1D). This metabolic disorder impairs two key cellular functions: hindered of energy generation due to impaired substrate utilization and disruption of biosynthetic pathways required for cell proliferation.[28] Specifically, the dual role of acetyl-CoA as both a lipid biosynthesis precursor and a central metabolic intermediate appears crucial for *B. subtilis* growth. These findings collectively demonstrate that PDH activity is essential for maintaining acetyl-CoA homeostasis, thereby confirming the enzyme's indispensable role in *B. subtilis* physiology.

The *pdhB* gene was not an optimal target for metabolic engineering. Therefore, we focused on pyruvate kinase (PYK). PYK irreversibly catalyzes the transfer of a phosphate group from PEP to ADP, generating pyruvate and ATP in the final step of glycolysis.[29] As shown in Figure 1B, the knockout of *pyk* in *B. subtilis* CGF-PC2 partially inhibited cellular growth, while the production of fengycin increased to 925.51 mg/L, representing a 47% increase compared to CGF-PG. The PEP content was elevated during the fermentation of strain CGF-PC2 compared with CGF-PG (Figure 1E), and the pyruvate level was maintained at a high level during 24−72 h (Figure 1D). Similar results were obtained in the studies of Heidarian[30] and Tang,[31] respectively, where glycolytic intermediates upstream of pyruvate accumulated in *pyk* mutants but pyruvate levels remained unchanged, and they suggested that this could be due to the limited effect of pyruvate kinase deficiency on pyruvate levels or the presence of other compensatory mechanisms. Heidarian et al. found by metabolomics that the fermentation products lactate and proline were reduced, confirming that larval metabolism is able to maintain pyruvate levels through the regulation of other compensatory pathways.[30] The blockage of the glycolysis pathway may redirect PEP toward the shikimate pathway,[32] boosting aromatic amino acid precursors for fengycin biosynthesis. The elevation of pyruvate content facilitated the accumulation of precursors necessary for fengycin synthesis. It is likely that pyruvate produced through PTS maintains bacterial growth, achieving a critical balance between metabolic rewiring and yield enhancement.[33] These results empirically validate the growth-product trade-off theory, demonstrating that strategic flux redistribution at key nodal points can optimize secondary metabolite synthesis without complete growth abolition.

Phosphoenolpyruvate carboxykinase (PckA) is essential for efficient gluconeogenesis from TCA cycle intermediates.[34] Knockout of the *pckA* gene disrupted oxaloacetate synthesis, resulting in a 10.4% increase in β-alanine production.[35] The *pckA* knockout reduced biomass (Figure 1B). However, fengycin production in strain CGF-PC3 showed no significant enhancement (Figure 1C). This may be attributed to the inactivity of the gluconeogenesis pathway under glucose-replete conditions.[34] Similarly, fengycin production in the double-knockout strain CGF-PC2C3 (Δ*pyk*, Δ*pckA*) showed no significant difference compared to strain CGF-PC2 (Δpyk) (Figure 1C). This could be explained by two factors: (1) the *pyk* knockout already minimized byproduct formation in central carbon metabolism, and (2) gluconeogenesis remained inactive due to excess glucose availability.

Fructose-1,6-bisphosphate kinase (PFK) plays a critical role in regulating carbohydrate metabolism, and its activity is an indicator glycolytic flux in microorganisms.[36] The *pfkA* gene was overexpressed using the P43 promoter to enhance carbon flux from upstream metabolic pathways and improve growth capacity. Overexpression of *pfkA* alone (strain CGF-PC4) significantly improved both cell growth (Figure 1B) and fengycin production (Figure 1C), with the fengycin production reaching 751.65 mg/L, representing a 19% increase compared to strain CGF-PG. However, the production improvement from

https://doi.org/10.1021/acssynbio.5c00101
ACS Synth. Biol. 2025, 14, 2644−2656

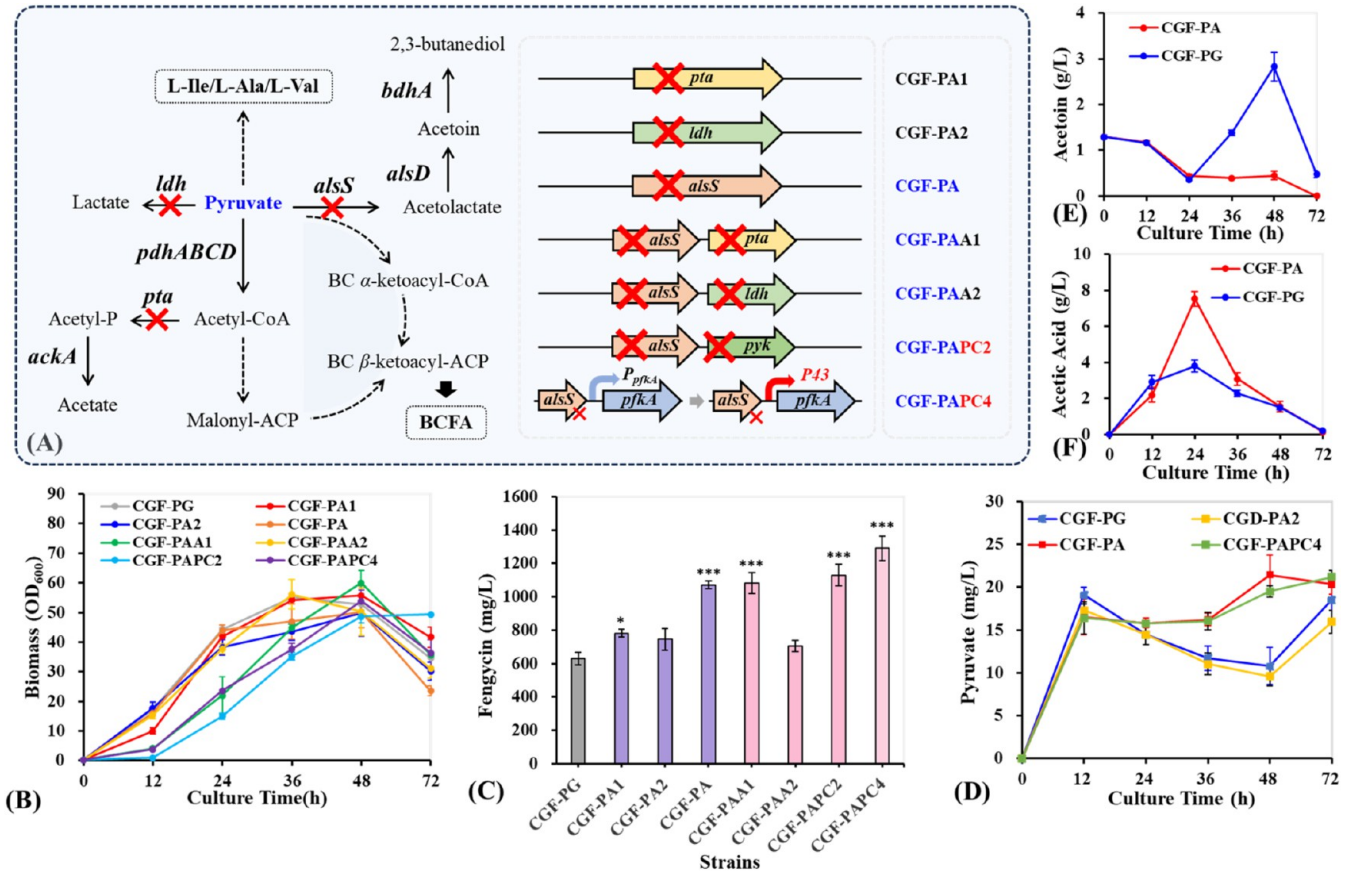

Figure 2. Effect of blocking the carbon overflow pathway on fengycin production. (A) Diagram of byproducts of central carbon metabolism. Red crosses (×) indicate gene knockouts. BCFA: branched-chain fatty acids. (B) Biomass (OD_{600}) of recombinant *B. subtilis*. (C) Fengycin production by recombinant *B. subtilis*. (D) Pyruvate production. (E) Acetoin production. (F) Acetic acid production. * $p < 0.05$, ** $p < 0.01$, *** $p < 0.001$.

pfkA overexpression was less significant than that achieved by *pyk* knockout, supporting the feasibility of enhancing fengycin production through growth suppression strategies. Notably, excessive activation of central metabolic pathways may lead to carbon source waste.[37] To optimize this, the strain CGF-PC3PC4 was further constructed by knocking out *pckA*, resulting in a 31% increase in fengycin production (981.10 mg/L) compared to strain CGF-PC4. This enhancement may be attributed to accelerated glucose consumption (due to reinforced central carbon metabolism) and blockage of gluconeogenesis (via *pckA* knockout), thereby reducing futile carbon and energy dissipation.[9]

Central carbon metabolism plays a critical role for microbial physiology, with genes such as *pyk*, *pdhABCD*, *pfkA*, and *pckA* encode key regulatory enzymes. Optimizing modifications in central metabolism to balance cellular growth and product synthesis while improving energy efficiency is a major goal of metabolic engineering.[38,39] Strategies such as partial pathway attenuation or dynamic regulation (rather than complete gene knockout) can effectively mitigate growth defects while maintaining production.[40] For example, deleting *pyk* minimally affects growth but enhances product yield, while inactivating *pdhB* severely impairs growth and reduces yield. Overexpression of genes in central carbon metabolism may differentially affect metabolite synthesis. Primary metabolites often show increased yields due to enhanced precursor supply,[41] whereas secondary metabolites may not benefit proportionally. Balancing carbon flux between glycolysis and gluconeogenesis is a promising strategy to optimize fengycin production.[42]

3.2. Impact of Blocking the Carbon Overflow Pathway in *B. subtilis*.

Knockout of competitive pathways is a common metabolic engineering strategy to enhance product production. During glucose utilization, major byproducts include acetic acid, acetoin, lactic acid, and 2,3-butanediol (Figure 2A).

Acetate synthesis from acetyl-CoA involves phosphotransacetylase (encoded by *pta*) and acetate kinase.[43] In aerobic glucose-defined media, eliminating the acetate pathway minimally affects growth or product production (Figure 2B). As shown in Figure 2C, the *pta* knockout strain CGF-PA1 increased fengycin production to 782.49 mg/L. Lactate dehydrogenase (*ldh*) catalyzes pyruvate reduction to lactate, wasting carbon flux and reducing equivalents.[44] The *ldh* knockout strain CGF-PA2 produced 746.76 mg/L, which was not significantly different from that of strain CGF-PG (Figure 2C). Meanwhile its pyruvate content during fermentation was the same as strain CGF-PG levels (Figure 2D).

In *B. subtilis*, α-acetolactate synthase (*alsS*) converts pyruvate to α-acetolactate, which is decarboxylated by α-acetolactate decarboxylase (*alsD*) to acetoin.[45] The *alsS* knockout strain CGF-PA showed minimal growth impact (Figure 2B), consistent with prior studies.[46] However, this led to a surge in fengycin production to 1071.11 mg/L, representing a 70% increase compared to strain CGF-PG (Figure 2C). This increase is likely due to the redirected carbon flux from acetoin overflow toward fengycin precursors. Acetoin synthesis may be the main carbon source leakage pathway in *B. subtilis*, and blocking its synthesis facilitates pyruvate accumulation. As shown in Figure 2D, its pyruvate content maintained a high level in the middle

https://doi.org/10.1021/acssynbio.5c00101
ACS Synth. Biol. 2025, 14, 2644−2656

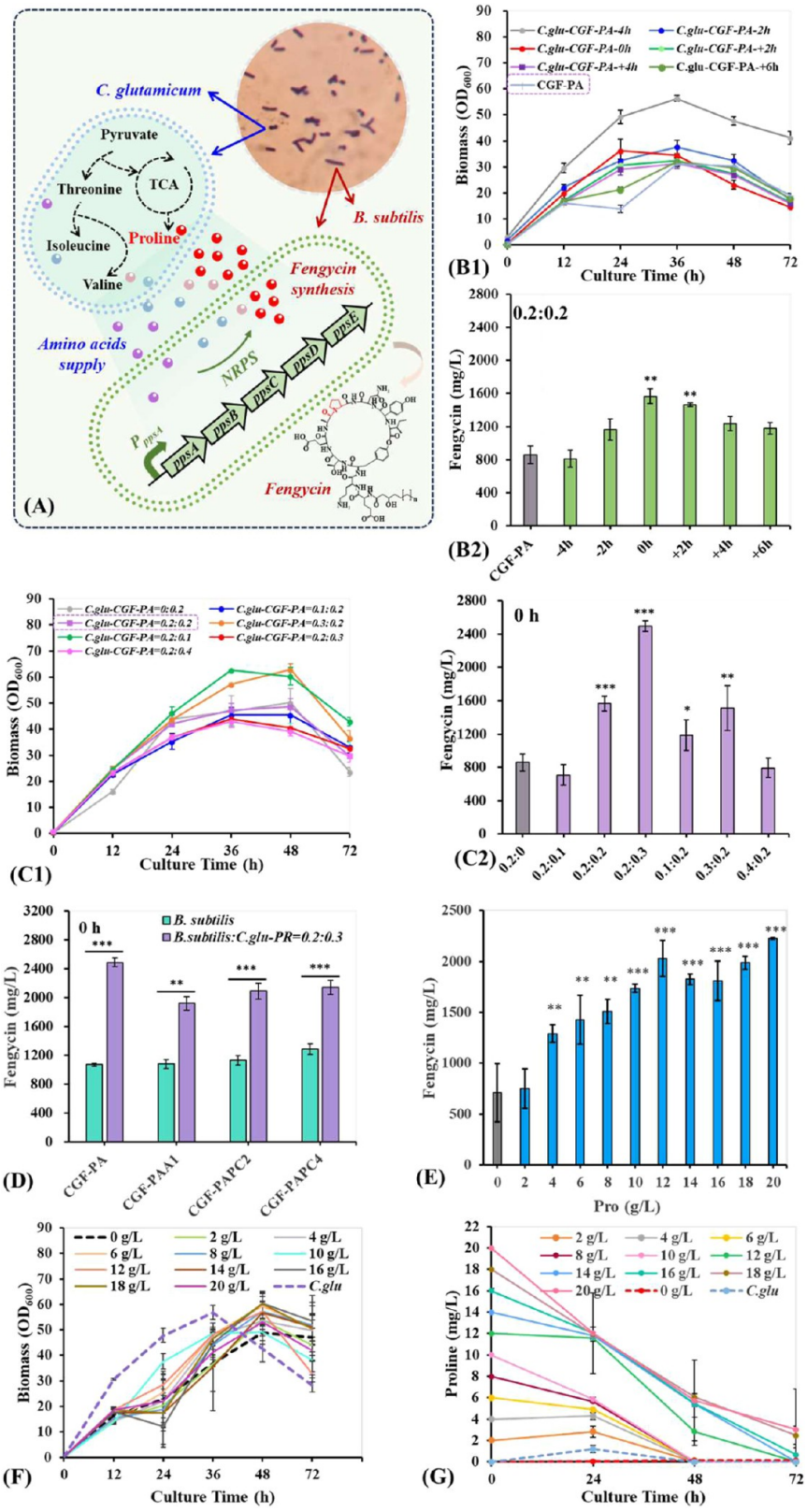

Figure 3. Construction of an artificial consortium of recombinant *B. subtilis* and *C. glu-PR*. (A) Schematic of coculture fermentation for fengycin production. (B1) Biomass (OD_{600}) of cocultures at different inoculation times. (−4 h: *C. glu-PR* inoculated 4 h earlier, −2 h: 2 h earlier, 0 h: simultaneously, + 2 h: 2 h later, + 4 h: 4 h later). (B2) Fengycin production at different inoculation times. (labels as in B1). (C1) Biomass (OD_{600}) at different inoculation ratios (*B. subtilis*: *C. glu-PR*): 0.2:0, 0.2:0.1, 0.2:0.2, 0.2:0.3, 0.1:0.2, 0.3:0.2, 0.4:0.2. (C2) Fengycin production at different inoculation ratios (labels as in C1). (D2) Fengycin production in coculture and monoculture. (E) Fengycin production with proline addition to Cal18−7 medium. (F) Biomass (OD_{600}) of Cal18−7 medium with proline addition. (G) Proline content in fermentation. * $p < 0.05$, ** $p < 0.01$, *** $p < 0.001$.

https://doi.org/10.1021/acssynbio.5c00101
ACS Synth. Biol. 2025, 14, 2644−2656

and late stages of fermentation simultaneously confirming this point. During the main synthesis period of fengycin (after 24 h of fermentation), the levels of acetic acid and acetoin in strain CGF-PA gradually decreased, while acetoin in strain CGF-PG was in the main synthesis stage (Figure 2E,F). Acetoin and acetic acid are generated from pyruvate and acetyl-CoA, respectively. The change in carbon source allocation resulting from the knockout of the acetoin synthesis pathway might be the reason for the increase in fengycin production.

Knocking out *pta*, *ldh*, or *alsS* can facilitate the accumulation of the pyruvate pool and acetyl-CoA, thereby promoting the production of precursor substances such as amino acids and fatty acids for fengycin synthesis.[47] The elimination of competing pathways contributes to the production of fengycin. However, dual knockouts did not exceed single-knockout production (Figure 2C). Single knockouts may have maximized the supply of key precursors (e.g., malonyl-CoA, amino acids), which could not be further increased by combining knockouts.[48]

Figure 2C illustrates that the strain CGF-PAPC4 (Δ*alsS*, P43-*pfkA*), achieved a further increase in fengycin production to 1290.31 mg/L, representing a 20% improvement over strain CGF-PA. It has been reported that the yield of pure cultured *B. subtilis* was 1400 mg/L, but its culture medium required the additional supplementation of a specific amino acid mixture.[7] As shown in Figure 2D, the pyruvate of CGF-PAPC4 was also at a high level. Additionally, the CGF-PAPC2 strain (Δ*alsS*, Δ*pyk*), showed a marginal production improvement. The slight increase in production may be due to the fact that the generation of acetoin is the most important overflow pathway from the central carbon source.

3.3. Co-Cultivation of *B. subtilis* and *C. glutamicum*. Co-cultivation is based on microbial interactions, including cross-feeding of metabolites and signaling molecule-mediated communication.[49] In the *B. subtilis* and *C. glutamicum* coculture system, strain *C. glu-PR* supplies proline for *B. subtilis* growth and fengycin synthesis (Figure 3A). The stability of the microbial community is regulated by adjusting the inoculation ratio and time during the fermentation process.

First, strains CGF-PA and *C. glu-PR* were cocultured at different inoculation intervals under an OD_{600} of 0.2 (strain *C. glu-PR* inoculated 4 h earlier, 2 h earlier, simultaneously, 2 h later, and 4 h later). To meet the growth requirements of *B. subtilis* and *C. glutamicum*, Cal18−7 medium was used as a substitute for Cal18 medium.[24] This change resulted in no increase in CGF-PA growth at 12−24 h (Figure 3B1) and a decrease in fengycin production of about 20%. As in Figure 3B2, simultaneous inoculation achieved the highest fengycin production (1564.89 mg/L), representing an 82% increase over monoculture. Extended inoculation intervals lowered fengycin production. This may be due to strain *C. glu-PR* becoming a dominant strain when inoculated earlier, thereby depleting the growth resources needed by *B. subtilis*. Alternatively, strain *C. glu-PR* may not have sufficient time to grow and produce proline for strain CGF-PA, leading to substrate competition with *B. subtilis* and resulting in a decrease in production.

Regarding the inoculation ratios, this study investigated the fermentation processes of strains CGF-PA and *C. glu-PR* at the following ratios under OD_{600}: 0.2:0, 0.2:0.1, 0.2:0.2, 0.2:0.3, 0.1:0.2, 0.3:0.2, and 0.4:0.2. Groups with higher biomass exhibited lower production (Figure 3C1), consistent with results from inoculation timing and monoculture experiments. From the fermentation results in Figure 3C2, simultaneous inoculation of CGF-PA and *C. glu-PR* at a ratio of 0.2:0.3 exhibited superior production capacity, with productivity reaching 2491.97 mg/L, which is approximately 190% higher than monoculture. Under the condition of two-strain mixed fermentation, the results of this experiment are superior to the previously reported 1220[7] and 1554.74 mg/L.[24]

Based on optimized fermentation conditions, high-production strains (CGF-PAA1, CGF-PAPC2, and CGF-PAPC4) were cocultured with strain *C. glu-PR* at a ratio of 0.2:0.3. Coculture systems outperformed monocultures (Figure 3D), though none exceeded strain CGF-PA's production. Coculture flexibility requires targeted optimization for stable consortia.[50]

In microbial coculture systems, it is hypothesized that cross-strain proline supply is the core driving force for enhancing fengycin biosynthesis.[24] However, the fermentation results from adding proline to the Cal18−7 medium showed the opposite effect. As shown in Figure 3E, when proline was added to the medium at concentrations ranging from 0 to 12 g/L, the fengycin yield gradually increased, but adding proline at higher concentrations did not significantly enhance the yield further. Figure 3F shows that the growth of strain CGF-PA did not improve during 12−24 h, the highest biomass of strain *C. glu*-PR was at 36 h, and the highest biomass of *B. subtilis* was delayed by 12 h. Figure 3G reveals the utilization of proline during fermentation: the proline produced by strain CGF-PA was very low, and the highest proline content produced by strain *C. glu*-PR in this medium was 1.2 g/L at 24 h. Based on proline content alone, the coculture system could not produce more fengycin. The coculture system clearly involves substance exchanges and molecular interactions beyond the designed parameters that promote fengycin production. Future research should employ multiomics approaches to reveal these cooperative mechanisms, thereby establishing fundamental principles for the rational design of synthetic microbial consortia in bioproduction applications.

3.4. Mass Spectrometry Analysis of Fengycin Produced by *B. subtilis*. To identify antifungal compounds in fermentation, the fengycin produced by CGF-PA was separated, purified, and analyzed by IMS-MS. Each component was characterized by matching its mass spectrometry data with previously reported fengycin structures. The IMS-MS spectra for all analyzed compounds are provided in Figures S1 to S12.

According to the results in Table 1, nine distinct fengycin components were identified in the purified sample. Components 1, 2, and 9 exhibited characteristic m/z values of 966.4878 and 1080.5681, corresponding to fengycin A. Based on molecular ion peaks, they were identified as C16 fengycin A, C17 fengycin A, and C17 fengycin A with one unsaturated bond in the fatty acid chain. Components 3 and 4 showed peaks at m/z 980.5071/980.5026 and 1094.5884, matching fengycin B2 and fengycin S.[51,52] Component 3 is tentatively assigned as C16 fengycin S or C15-fengycin B2, while component 4 is likely C18 fengycin S or C17 fengycin B2. Component 5 displayed peaks at m/z 1008.6672 and 1022.7021, consistent with fengycin C. The molecular ion peak at m/z 1491.8809 suggested it is C17 fengycin C. Components 6, 7, and 8 had peaks at m/z 994.5258/994.5211/994.5119 and 1108.6113/1108.5919. And they were hypothesized as C19 fengycin B, C18 fengycin B, and C15 fengycin B, respectively.

In the unpurified mixture, additional fengycin variants were detected. A component matching fengycin A with a molecular ion peak at m/z 1449.8267 was identified as C15-fengycin A. Peaks at m/z 1491.8695 and 1489.8844 corresponded to

https://doi.org/10.1021/acssynbio.5c00101
ACS Synth. Biol. 2025, 14, 2644−2656

Table 1. Mass Spectral Results of Each Component in This Study

	M/Z	detected characteristic ion peaks	types
component 1	1463.8433	1080.5681, 966.4878	C16 fengycin A
component 2	1477.8579	1080.5681, 966.4878	C17 fengycin A
component 3	1478.8632	1094.5884, 980.5071	C16 fengycin S/C15 fengycin B2
component 4	1506.9012	1094.5884, 980.5026	C18 fengycin S/C17 fengycin B2
component 5	1491.8809	1022.7021, 1008.6672	C17 fengycin C
component 6	1520.9160	1108.6113, 994.5258	C19 fengycin B
component 7	1506.9070	1108.6113, 994.5211	C18 fengycin B
component 8	1476.8794	1108.5919, 994.5119	C15 fengycin B
component 9	1475.8936	1080.5729, 966.4923	C17 fengycin A (unsaturated)
other component	1449.8267	1080.5729, 966.4923	C15 fengycin A
other component	1491.8695	1108.5919, 994.5119	C16 fengycin B (saturated)
other component	1489.8844	1108.5919, 994.5119	C16 fengycin B (unsaturated)

fengycin B, likely representing C16-fengycin B with a saturated or unsaturated fatty acid chain.

3.5. Antifungal Activity of Fengycin Produced by *B. subtilis*. *3.5.1. Effects of Fengycin Produced by B. subtilis. on Fungi.* In this study, *F. graminearum*, *B. cinerea*, *P. oryzae*, and *R. solani* were used as indicator fungi to evaluate the antifungal activity of fengycin extracts obtained from recombinant *B. subtilis*. The inhibitory effects of fengycin at different concentrations on four fungal strains are illustrated in Figure S13. The results demonstrate that, within the tested concentration range, higher fengycin concentrations were associated with stronger inhibitory effects on fungal growth.

F. graminearum is a notorious pathogen causing head blight in cereal crops, deteriorating grain quality and reducing crop production. Fengycin has been shown to significantly inhibit its growth.[53] Under normal conditions, *F. graminearum* reaches a diameter of 5 cm in 4 days, but on PDA plates supplemented with 50 mg/L fengycin, this took 6 days. The longer the cultivation time, the more pronounced the differences in colony size (Figure 4A1). Moreover, there were significant changes in the colony morphology. In the control group, the mycelium was dense, and the fungal layer was thick, with vibrant red pigmentation on the PDA plate underside. In contrast, the experimental group exhibited loose mycelium, a noticeably thinner fungal layer, and a white underside (Figure 4A2). Fengycin effectively inhibited the growth of *F. graminearum*.

Root rot caused by *R. solani* is a global agricultural threat. Fengycin disrupts the *R. solani* cell wall, inducing vacuolation, protoplasm leakage, and hyphal deformation (irregular growth, twisting, and fragmentation).[54] Although *R. solani* grew vigorously, it required 2 additional days to reach 5 cm on fengycin-supplemented PDA plates compared to untreated controls (Figure 4B1). In the control group, *R. solani* exhibited white, dense mycelium. However, on fengycin-supplemented PDA plates, hyphae became denser with upward growth tendencies and a thickened fungal layer (Figure 4B2).

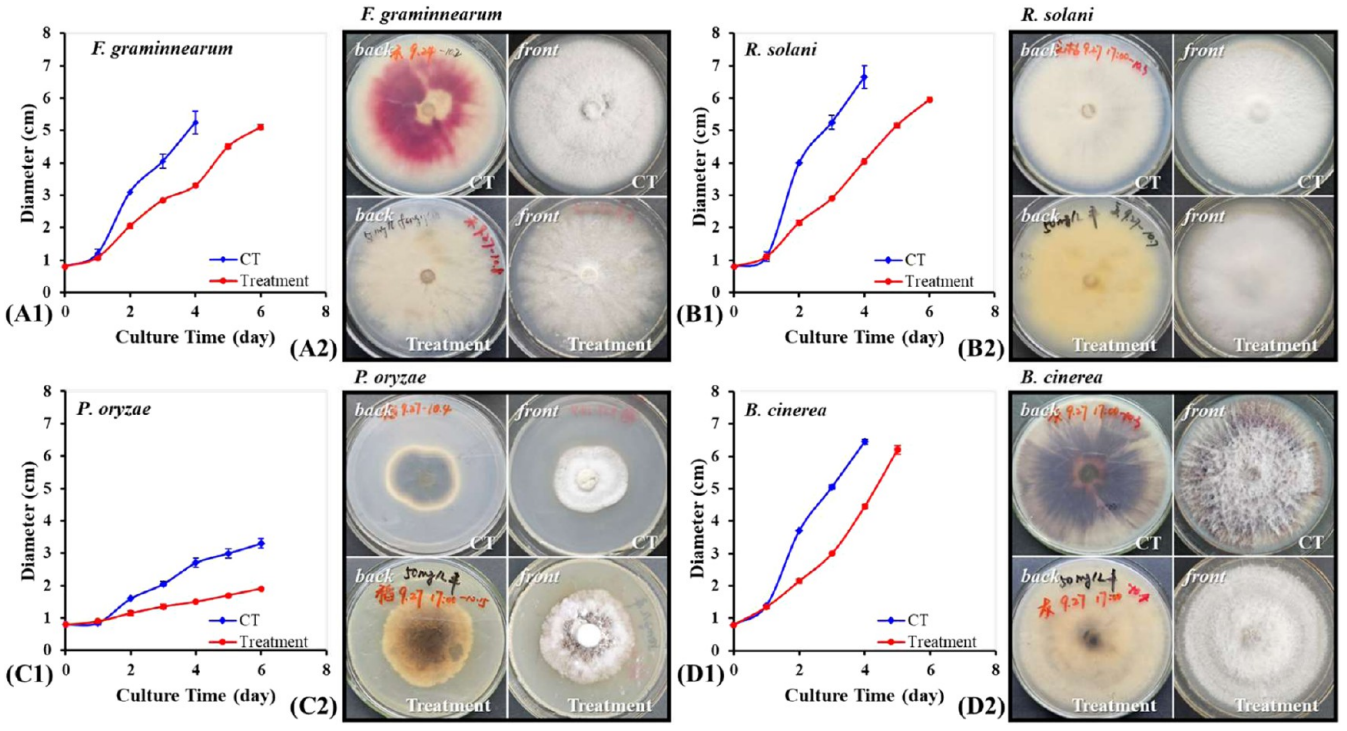

Figure 4. Antifungal effects of fengycin from recombinant *B. subtilis* CGF-PA against different fungal. (A1) The growth diameters of *F. graminearum* under the treatment and CT; (A2) *F. graminearum* appearance from different perspectives. (B1) The growth diameter of *R. solani* under the treatment and CT. (B2) *R. solani* appearance from different perspectives. (C1) The growth diameter of *P. oryzae* under the treatment and CT. (C2) *P. oryzae* appearance from different perspectives of the control group and experimental group. (D1) The growth diameter of *B. cinerea* under the treatment and CT. (D2) *B. cinerea* appearance from different perspectives of the control group and experimental group. CT: PDA agar plate. Treatment: PDA agar plate with 50 mg/L fengycin. Variations in culture days arise from smaller Petri dishes and fungi's differential growth in distinct environments.

https://doi.org/10.1021/acssynbio.5c00101
ACS Synth. Biol. 2025, 14, 2644−2656

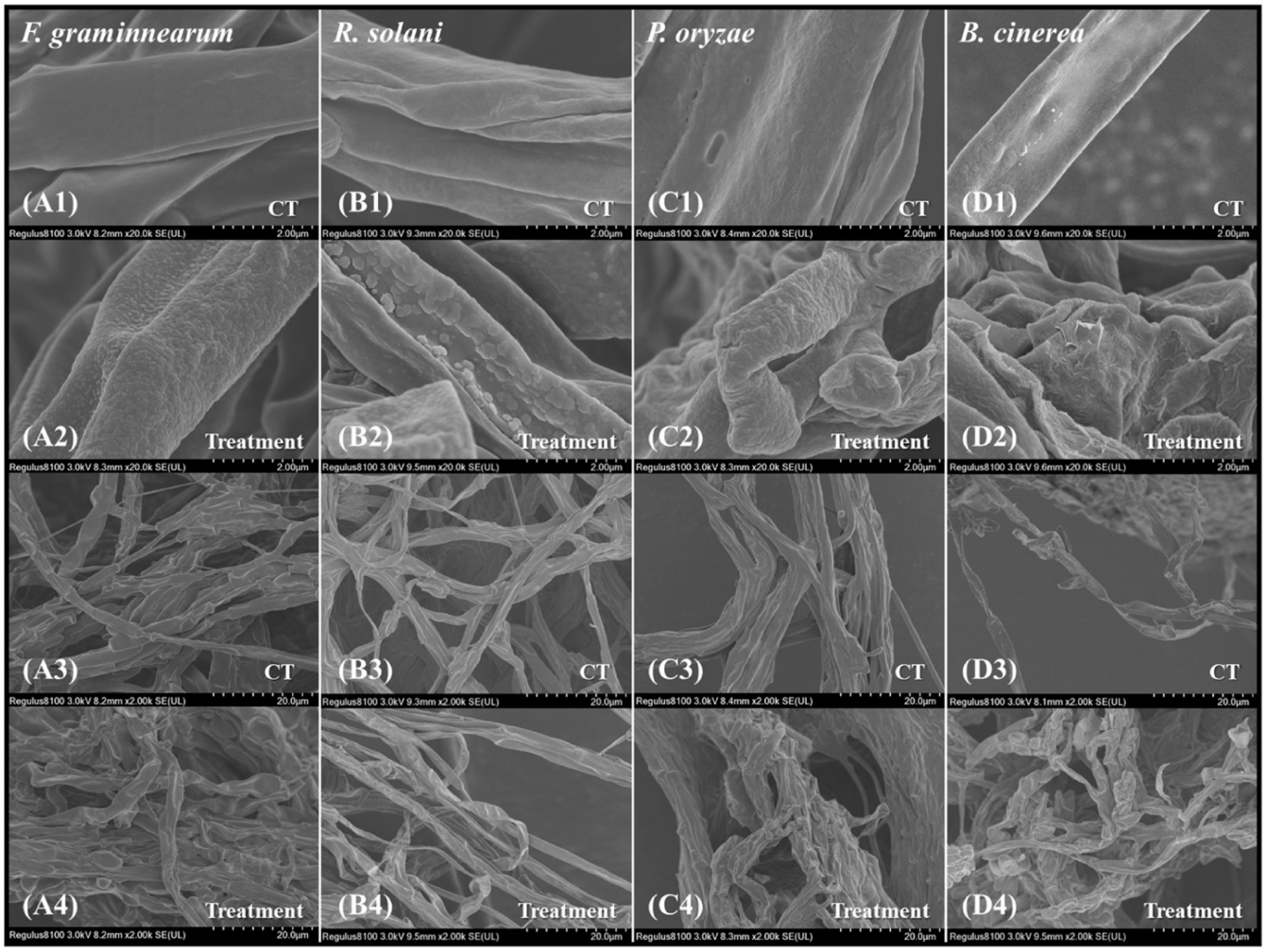

Figure 5. Effect of fengycin (50 mg/L) on different fungal hyphae. (A1)−(A4) SEM comparison images of *F. graminearum.* (B1)−(B4) SEM comparison images of *R. solani.* (C1)−(C4) SEM comparison images of *P. oryzae.* (D1)−(D4) SEM comparison images of *B. cinerea.* CT: mycelium from PDA agar plate. Treatment: mycelium from PDA agar plate with 50 mg/L fengycin.

Rice blast disease caused by *P. oryzae* is highly destructive, drastically reducing rice yields. Fengycin, a potent lipopeptide, inhibits *P. oryzae* by deforming conidia and germ tubes and suppressing mycelial growth.[55] As shown in Figure 4C1, *P. oryzae* growth was significantly slower on fengycin-containing plates. To reach a target diameter of 1.5 cm, a 2-day delay was observed, with colony size disparities becoming more pronounced over time. *P. oryzae* showed significant differences on PDA plates with and without fengycin. In the control group, the mycelium was pure white with dark blue-black pigmentation on the plate underside; in the experimental group, the hyphal layer near the center appeared pale yellow and shriveled, and the underside showed brownish-yellow pigmentation (Figure 4C2).

Botrytis bunch rot, caused by the necrotrophic fungal pathogen *B. cinerea*, is a major disease of grapevines. Infection of mature berries significantly reduces the quantity and quality of both table and wine grapes under field and postharvest conditions. However, colonization by *Bacillus* strains harboring fengycin gene clusters can prevent *B. cinerea* entry and proliferation.[56] *B. cinerea* exhibited rapid growth at 30 °C, but 50 mg/L fengycin significantly inhibited its growth rate compared to other antifungal agents (Figure 4D1). After 2 days of cultivation, the difference in colony diameter between the experimental and control groups reached approximately 2 cm and remained stable thereafter, suggesting that fengycin primarily suppresses early stage hyphal expansion. While *B. cinerea* colonies typically display a purple pigmentation, fengycin treatment induces decolorization, resulting in white mycelial mats and pale reverse sides of the colonies (Figure 4D2).

The fungal growth in the experimental group was markedly slower than in the control, demonstrating fengycin's inhibitory effect on all four tested fungal species. And fengycin is selective in its inhibitory effect on different fungi, as shown in previous studies.[57] Treated colonies exhibited morphological alterations, including denser or sparser mycelial networks and increased aggregation, which hindered expansion. Decolorization was also observed. These findings align with SEM analyses (Figure 5), revealing that untreated hyphae had smooth surfaces and tightly interwoven structures, whereas fengycin-treated hyphae (50 mg/L) showed severe deformations, such as surface depressions, swelling, and wrinkling. Similar morphological disruptions, including irregular pores and collapsed structures, have been reported in prior studies.[53,58,59]

3.5.2. Different Antifungal Effects of Fengycin Homologues. Most antifungal studies have focused on fengycin as a broad-spectrum mixture.[60] However, liquid chromatography profiles revealed distinct distributions of fengycin components among *Bacillus* strains CGF-PA, CGF-PG, and CGF-PVSF

https://doi.org/10.1021/acssynbio.5c00101
ACS Synth. Biol. 2025, 14, 2644−2656

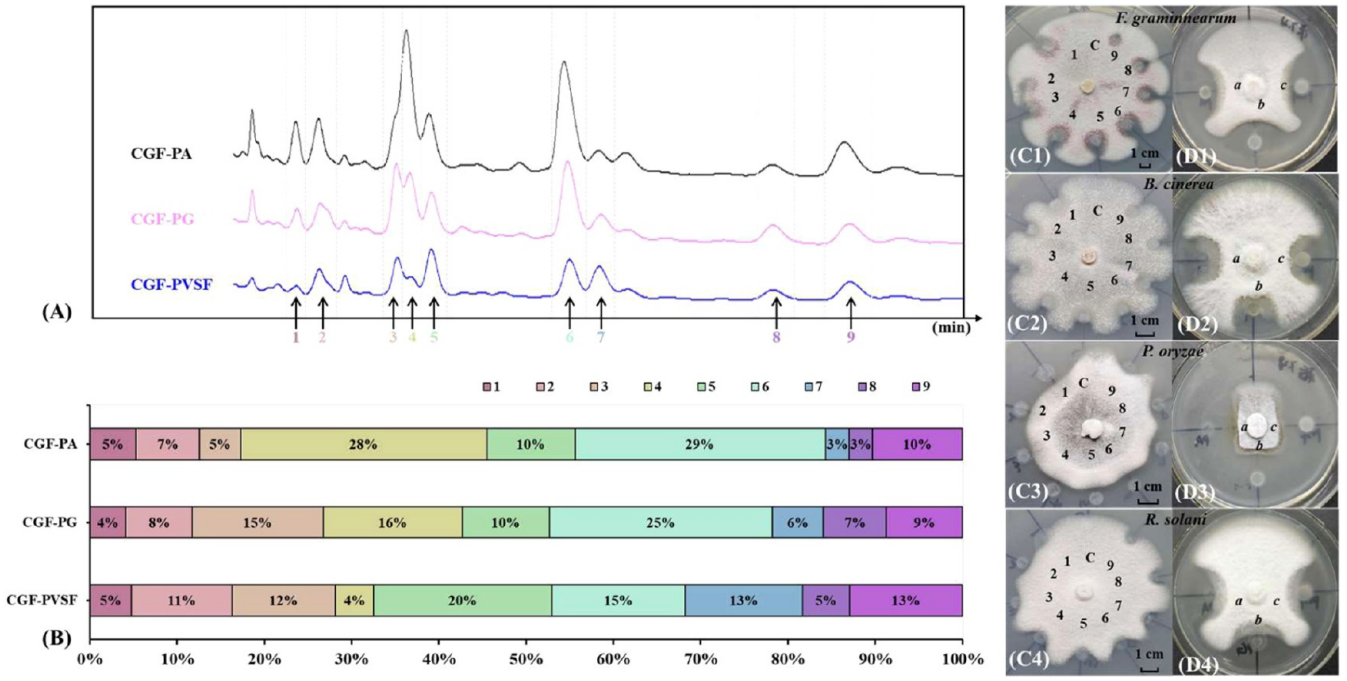

Figure 6. Antifungal activity and isoform distribution of fengycin. (A) HPLC profiles of fengycin produced by *Bacillus* strains CGF-PA, CGF-PG, and CGF-PVSF. (B) Proportional abundance of fengycin isoforms in each strain. (C1) - (C4) Antifungal activity of nine fengycin components against *F. graminearum*, *B. cinerea*, *P. oryzae*, and *R. solani*. Components 1−9 are labeled as follows:1: C16 fengycin A; 2: C17 fengycin A; 3: C16 fengycin S/C15 fengycin B2; 4: C18 fengycin S/C17 fengycin B2; 5: C17 fengycin C; 6: C19 fengycin B; 7: C18 fengycin B; 8: C15 fengycin B; 9: C17 fengycin A (unsaturation). (D1) - (D4) Antifungal activity of fengycin produced by recombinant *B. subtilis* strains against the four fungi. Strains: a (CGF-PA), b (CGF-PG), c (CGF-PVSF).

(Figure 6A, B). At a low concentration (50 mg/L), the antifungal efficacy of individual isoforms varied significantly across fungal species (Figure 6C). Antifungal ability was reflected in the size of the inhibitory zone.

Among the same fungal strains, different components exhibited slight variations in their inhibitory effects, with the differences in inhibition against *F. graminearum* and *P. oryzae* being the most pronounced. For *F. graminearum* (Figure 6C1), components 5 and 6 exhibited the strongest activity, while components 1, 2, 3, 8, and 9 showed weak inhibition. Components 3, 8, and 9 also displayed reduced activity against *B. cinerea* (Figure 6C2). For *P. oryzae* (Figure 6C3) and *R. solani* (Figure 6C4), components 8 and 9 were less effective compared to others. Overall, components 2 (C17 fengycin A), 8 (C15 fengycin B), and 9 (C17 fengycin A (unsaturation)) were relatively weak in their antifungal capabilities. Component 1 (C16 fengycin A) demonstrated a strong antifungal effect against *P. oryzae*. Component 3 (C16 fengycin S or C15 fengycin B2) exhibited weaker inhibition against *B. cinerea* and *F. graminearum* compared to its inhibitory effect on *P. oryzae* and *R. solani*. Components 4 (C18 fengycin S or C17 fengycin B2), 5 (C17 fengycin C), 6 (C19 fengycin B), and 7 (C18 fengycin B) displayed similar and relatively strong antifungal activity. The fatty acid chains of lipopeptides are typically capable of penetrating the lipid bilayer and orienting themselves toward the interior, while the peptide ring remains on the surface, interacting with the lipid head groups. Structural analysis has revealed that the antifungal potency is related to electrostatic interactions between charged residues (such as glutamate and ornithine) and the lipid membrane.[22] Isoforms rich in anionic amino acids may enhance membrane disruption.[61] Botcazon et al. argue that, compared to PC, fengycin preferentially interacts with phosphatidylethanolamine (PE), possibly because the amino group of PE can act as a hydrogen bond donor, while the choline group of PC cannot, thus forming favorable interactions with the anionic side chains of the peptide. Phosphatidic acid (PA) may exert an electrostatic repulsion on fengycin, as fengycin contains two negatively charged glutamate residues and one positively charged ornithine residue, resulting in an overall charge of −1.[62] The C17−C19 fengycin (components 4−7) have longer fatty acid chains, allowing for deeper insertion into the fungal cell membrane through hydrophobic interactions, thereby disrupting membrane integrity. Compared to C15−C16 fatty acid chains (components 1, 3, 8), the shorter chains have weaker hydrophobicity and reduced membrane perturbation ability, leading to decreased activity, which is consistent with previous research findings. Deleu et al. found that the difference in fatty acid chain length during the interaction of fengycin with a monolayer of saturated phospholipid DPPC might be the cause of monolayer collapse.[21] Leconte et al. also suggested that within the same family, the length of the fatty acid chain can modulate biological activity.[63] Longer acyl chains can interact with the lipid membrane, and in many cases, the chain length determines their antimicrobial activity,[64] meaning longer chains generally correspond to stronger activity. The specific activity of component 1 against *P. oryzae* may originate from the unique membrane lipid composition of this pathogen, which favors interaction with medium-chain fengycin. The observed differences in antifungal effects among fengycin components stem from the structural differences in fatty acid chain length and amino acid composition, both of which jointly determine the efficiency of membrane interaction.

The strain CGF-PA produces the highest proportions of components 4, 5, 6, and 7, accounting for 74%, while strain

https://doi.org/10.1021/acssynbio.5c00101
ACS Synth. Biol. 2025, 14, 2644−2656

CGF-PG and CGF-PVSF account for 57% and 54%, respectively (Figure 6B). Interestingly, strain CGF-PA contains more components 4, 5, 6, and 7 with stronger antifungal properties, its overall antifungal performance is suboptimal. The proportions of fengycin in strains CGF-PVSF and CGF-PG correlate with comparable or stronger antifungal effects compared to strain CGF-PA (Figure 6D). This paradox may arise from component antagonism or environmental instability. In contrast, strains CGF-PVSF and CGF-PG achieved comparable efficacy with fewer potent components, implying synergistic effects or adaptive fitness trade-offs.[65] Further research is needed to unravel the mechanisms underlying fengycin's selective activity and optimize its application in biocontrol strategies.

The *B. subtilis* monoculture and *B. subtilis-C glutamicum* coculture systems developed in this study achieved high-level fengycin production, alongside in-depth investigations into the structure−activity relationships of fengycin variants. These findings provide a robust framework for optimizing fengycin yields and deciphering its antifungal mechanisms. In the future, we can further explore how to use inducible promoters to achieve the decoupling of the "growth-production" stage and balance the yield and cell adaptability. Fengycin synthase could be reconstituted by synthetic biology to produce highly active homologues and reduce inefficient variants. Molecular dynamics simulations could be used to predict the optimal combination of lipid chain length and charge distribution to guide enzyme engineering transformation. Large-scale fengycin production holds transformative potential for sustainable agriculture, medicine, and food preservation.

■ ASSOCIATED CONTENT

Supporting Information

The Supporting Information is available free of charge at https://pubs.acs.org/doi/10.1021/acssynbio.5c00101.

Fengycin characteristic fragment ions (Table S1), strains and plasmids used in this study (Table S2), primers used in this study (Table S3), IMS-MS spectra of all identified fengycin homologues (Figures S1−S12), and antifungal activity of fengycin at different concentrations (Figure S13) (PDF)

■ AUTHOR INFORMATION

Corresponding Authors

Qiu-Man Xu − *Tianjin Key Laboratory of Animal and Plant Resistance, College of Life Science, Tianjin Normal University, Tianjin 300387, P. R. China*; Email: qmxu0929@126.com

Jing-Sheng Cheng − *State Key Laboratory of Synthetic Biology, Tianjin University, Tianjin 300072, P. R. China; Frontiers Science Center for Synthetic Biology (Ministry of Education), School of Synthetic Biology and Biomanufacturing, Tianjin University, Tianjin 300350, P. R. China*; orcid.org/0000-0002-1788-9382; Email: jscheng@tju.edu.cn

Authors

Dun-Ju Wang − *State Key Laboratory of Synthetic Biology, Tianjin University, Tianjin 300072, P. R. China; Frontiers Science Center for Synthetic Biology (Ministry of Education), School of Synthetic Biology and Biomanufacturing, Tianjin University, Tianjin 300350, P. R. China*

Ming-Zhu Ding − *State Key Laboratory of Synthetic Biology, Tianjin University, Tianjin 300072, P. R. China; Frontiers Science Center for Synthetic Biology (Ministry of Education), School of Synthetic Biology and Biomanufacturing, Tianjin University, Tianjin 300350, P. R. China*; orcid.org/0000-0003-0349-5240

Zheng-Jie Hou − *State Key Laboratory of Synthetic Biology, Tianjin University, Tianjin 300072, P. R. China; Frontiers Science Center for Synthetic Biology (Ministry of Education), School of Synthetic Biology and Biomanufacturing, Tianjin University, Tianjin 300350, P. R. China*

Yong Zhang − *State Key Laboratory of Synthetic Biology, Tianjin University, Tianjin 300072, P. R. China; School of Mathematics, Tianjin University, Tianjin 300072, People's Republic of China*

Wei Shang − *State Key Laboratory of Synthetic Biology, Tianjin University, Tianjin 300072, P. R. China; Frontiers Science Center for Synthetic Biology (Ministry of Education), School of Synthetic Biology and Biomanufacturing, Tianjin University, Tianjin 300350, P. R. China*

Tian-Xu Duan − *State Key Laboratory of Synthetic Biology, Tianjin University, Tianjin 300072, P. R. China; Frontiers Science Center for Synthetic Biology (Ministry of Education), School of Synthetic Biology and Biomanufacturing, Tianjin University, Tianjin 300350, P. R. China*

Complete contact information is available at: https://pubs.acs.org/10.1021/acssynbio.5c00101

Author Contributions

⊥D.-J.W. and M.-Z.D. contributed equally to this work. D.-J.W.: Implementing experiments, data analysis, and writing—Original draft preparation. M.-Z.D.: Funding acquisition and writing—review and editing. Z.-J.H.: Providing experimental assistance and writing —review and editing. Y.Z.: Project administration and review [TC5]& editing. W.S.: Providing experimental assistance and writing—review and editing. T.-X.D.: Mass spectrometry experiment and data analysis. Q.-M.X.: Funding acquisition, project administration, and writing—review and editing. J.-S.C.: Funding acquisition, project administration, supervision, and writing—review and editing.

Notes

The authors declare no competing financial interest.

■ ACKNOWLEDGMENTS

The authors are grateful for the financial support from the National Key R&D Program of China (2024YFA0919000) and the National Natural Science Foundation of China (Program: 22478291, 21878224).

■ REFERENCES

(1) Samel, S. A.; Wagner, B.; Marahiel, M. A.; Essen, L. The thioesterase domain of the fengycin biosynthesis cluster: a structural base for the macrocyclization of a non-ribosomal lipopeptide. *J. Mol. Biol.* **2006**, *359* (4), 876−889.

(2) Tao, Y.; Bie, X.; Lv, F.; Zhao, H.; Lu, Z. Antifungal activity and mechanism of fengycin in the presence and absence of commercial surfactin against *Rhizopus stolonifer*. *J. Microbiol.* **2011**, *49* (1), 146−150.

(3) Dey, G.; Bharti, R.; Sen, R.; Mandal, M. Microbial amphiphiles: a class of promising new-generation anticancer agents. *Drug Discovery Today* **2015**, *20* (1), 136−146.

(4) Kang, B. R.; Park, J. S.; Jung, W. Antiviral activity by lecithin-induced fengycin lipopeptides as a potent key substrate against *Cucumber mosaic virus*. *Microb. Pathog.* **2021**, *155*, No. 104910.

(5) Hmidet, N.; Ben Ayed, H.; Jacques, P.; Nasri, M. Enhancement of surfactin and fengycin production by *Bacillus mojavensis* A21:

application for diesel biodegradation. *Biomed Res. Int.* **2017**, *2017* (1), No. 5893123.
(6) Yin, Y.; Wang, X.; Zhang, P.; Wang, P.; Wen, J. Strategies for improving fengycin production: a review. *Microb. Cell. Fact.* **2024**, *23*, 144.
(7) Wei, S.-Y.; Gao, G.; Ding, M.; Cao, C.; Hou, Z.; Cheng, J.; Yuan, Y. An engineered microbial consortium provides precursors for fengycin production by *Bacillus subtilis*. *J. Nat. Prod.* **2024**, *87* (1), 28−37.
(8) Matsuoka, Y.; Shimizu, K. Importance of understanding the main metabolic regulation in response to the specific pathway mutation for metabolic engineering of *Escherichia coli*. *Comp. Struct. Biotechnol. J.* **2012**, *3*, No. e201210018.
(9) Sauer, U.; Eikmanns, B. J. The PEP-pyruvate-oxaloacetate node as the switch point for carbon flux distribution in bacteria. *FEMS Microbiol. Rev.* **2005**, *29* (4), 765−794.
(10) Wu, F.; Wang, S.; Zhou, D.; Gao, S.; Song, G.; Liang, Y.; Wang, Q. Metabolic engineering of *Escherichia coli* for high-level production of the biodegradable polyester monomer 2-pyrone-4,6-dicarboxylic acid. *Metab. Eng.* **2024**, *83*, 52−60.
(11) Maughan, H.; Nicholson, W. L. Increased fitness and alteration of metabolic pathways during *Bacillus subtilis* evolution in the laboratory. *Appl. Environ. Microbiol.* **2011**, *77* (12), 4105−4118.
(12) Valdés-Velasco, L. M.; Favela-Torres, E.; Théatre, A.; Arguelles-Arias, A.; Saucedo-Castañeda, J. G.; Jacques, P. Relationship between lipopeptide biosurfactant and primary metabolite production by *Bacillus strains* in solid-state and submerged fermentation. *Bioresour. Technol.* **2022**, *345*, No. 126556.
(13) Cochrane, S. A.; Vederas, J. C. Lipopeptides from *Bacillus* and *Paenibacillus spp.*: a gold mine of antibiotic candidates. *Med. Res. Rev.* **2016**, *36* (1), 4−31.
(14) Yang, H.; Li, X.; Li, X.; Yu, H.; Shen, Z. Identification of lipopeptide isoforms by MALDI-TOF-MS/MS based on the simultaneous purification of iturin, fengycin, and surfactin by RP-HPLC. *Anal. Bioanal. Chem.* **2015**, *407* (9), 2529−2542.
(15) Wang, J.; Liu, J.; Wang, X.; Yao, J.; Yu, Z. Application of electrospray ionization mass spectrometry in rapid typing of fengycin homologues produced by *Bacillus subtilis*. *Lett. Appl. Microbiol.* **2004**, *39* (1), 98−102.
(16) Wang, R.; Zhao, S.; Wang, Z.; Koffas, M. A. Recent advances in modular co-culture engineering for synthesis of natural products. *Curr. Opin. Biotechnol.* **2020**, *62*, 65−71.
(17) Liu, Y.; Lu, J.; Sun, J.; Lu, F.; Bie, X.; Lu, Z. Membrane disruption and DNA binding of *Fusarium graminearum* cell induced by c16-fengycin a produced by *Bacillus amyloliquefaciens*. *Food Control* **2019**, *102*, 206−213.
(18) Guo, Q.; Dong, W.; Li, S.; Lu, X.; Wang, P.; Zhang, X.; Wang, Y.; Ma, P. Fengycin produced by *Bacillus subtilis* NCD-2 plays a major role in biocontrol of cotton seedling damping-off disease. *Microbiol. Res.* **2014**, *169* (7−8), 533−540.
(19) Lam, V. B.; Meyer, T.; Arias, A. A.; Ongena, M.; Oni, F. E.; Höfte, M. *Bacillus* cyclic lipopeptides iturin and fengycin control rice blast caused by *Pyricularia oryzae* in potting and acid sulfate soils by direct antagonism and induced systemic resistance. *Microorganisms* **2021**, *9* (7), 1441.
(20) Zhou, L.; Song, C.; Muñoz, C. Y.; Kuipers, O. P. *Bacillus cabrialesii* BH5 protects tomato plants against *Botrytis cinerea* by production of specific antifungal compounds. *Front. Microbiol.* **2021**, *12*, No. 707609.
(21) Deleu, M.; Paquot, M.; Nylander, T. Fengycin interaction with lipid monolayers at the air-aqueous interface-implications for the effect of fengycin on biological membranes. *J. Colloid Interface Sci.* **2005**, *283* (2), 358−365.
(22) Sur, S.; Romo, T. D.; Grossfield, A. Selectivity and mechanism of fengycin, an antimicrobial lipopeptide, from molecular dynamics. *J. Phys. Chem. B* **2018**, *122* (8), 2219−2226.
(23) Gao, G.-R.; Hou, Z.; Ding, M.; Bai, S.; Wei, S.; Qiao, B.; Xu, Q.; Cheng, J.; Yuan, Y. Improved production of fengycin in *Bacillus subtilis* by integrated strain engineering strategy. *ACS Synth. Biol.* **2022**, *11* (12), 4065−4076.
(24) Gao, G.-R.; Wei, S.; Ding, M.; Hou, Z.; Wang, D.; Xu, Q.; Cheng, J.; Yuan, Y. Enhancing fengycin production in the co-culture of *Bacillus subtilis* and *Corynebacterium glutamicum* by engineering proline transporter. *Bioresour. Technol.* **2023**, *383*, No. 129229.
(25) Cheng, Y.; Lou, H.; He, H.; He, X.; Wang, Z.; Gao, X.; Liu, J. Genomic and biological control of *Sclerotinia sclerotiorum* using an extracellular extract from *Bacillus velezensis* 20507. *Front. Microbiol.* **2024**, *15*, No. 1385067.
(26) Wang, X.-F.; Miao, C.; Qiao, B.; Xu, S.; Cheng, J. Co-culture of *Bacillus amyloliquefaciens* and recombinant *Pichia pastoris* for utilizing kitchen waste to produce fengycins. *J. Biosci. Bioeng.* **2022**, *133* (6), 560−566.
(27) Qian, J.; Wang, Y.; Liu, X.; Hu, Z.; Xu, N.; Wang, Y.; Shi, T.; Ye, C. Improving acetoin production through construction of a genome-scale metabolic model. *Comput. Biol. Med.* **2023**, *158*, No. 106833.
(28) Kozak, B. U.; van Rossum, H. M.; Luttik, M. A. H.; Akeroyd, M.; Benjamin, K. R.; Wu, L.; de Vries, S.; Daran, J.; Pronk, J. T.; van Maris, A. J. A. Engineering acetyl coenzyme a supply: functional expression of a bacterial pyruvate dehydrogenase complex in the cytosol of *Saccharomyces cerevisiae*. *mBio* **2014**, *5* (5), e01614−e01696.
(29) Horemans, S.; Pitoulias, M.; Holland, A.; Pateau, E.; Lechaplais, C.; Ekaterina, D.; Perret, A.; Soultanas, P.; Janniere, L. Pyruvate kinase, a metabolic sensor powering glycolysis, drives the metabolic control of DNA replication. *BMC Biol.* **2022**, *20* (1), 87.
(30) Heidarian, Y.; Tourigny, J. P.; Fasteen, T. D.; Mahmoudzadeh, N. H.; Hurlburt, A. J.; Nemkov, T.; Reisz, J. A.; D'Alessandro, A.; Tennessen, J. M. Metabolomic analysis of drosophila melanogaster larvae lacking pyruvate kinase. *G3* **2023**, *14* (1), No. jkad228.
(31) Tang, B.; Xue, K. S.; Wang, J.; Williams, P. L.; Tang, L. Bacteria pyruvate metabolism modulates AFB_1 toxicity in *Caenorhabditis* elegans. *Sci. Total Environ.* **2023**, *900*, No. 165809.
(32) Shen, Y.-P.; Niu, F.; Yan, Z.; Fong, L. S.; Huang, Y.; Liu, J. Recent advances in metabolically engineered microorganisms for the production of aromatic chemicals derived from aromatic amino acids. *Front. Bioeng. Biotechnol.* **2020**, *8*, 407.
(33) Fry, B.; Zhu, T.; Domach, M. M.; Koepsel, R. R.; Phalakornkule, C.; Ataai, M. M. Characterization of growth and acid formation in a *Bacillus subtilis* pyruvate kinase mutant. *Appl. Environ. Microbiol.* **2000**, *66* (9), 4045−4049.
(34) Servant, P.; Le Coq, D.; Aymerich, S. CcpN (YqzB), a novel regulator for CcpA-independent catabolite repression of *Bacillus subtilis* gluconeogenic genes. *Mol. Microbiol.* **2005**, *55* (5), 1435−1451.
(35) Yang, S.; Li, J.; Meng, R.; Yu, T.; Wang, Z.; Xiong, P.; Gao, Z. Screening and identification of genes involved in β-alanine biosynthesis in *Bacillus subtilis*. *Arch. Biochem. Biophys.* **2023**, *743*, No. 109664.
(36) Muñoz-Márquez, M.; Ponce-Rivas, E. Effect of *pfkA* chromosomal interruption on growth, sporulation, and production of organic acids in *Bacillus subtilis*. *J. Basic Microbiol.* **2010**, *50* (3), 232−240.
(37) Gu, Y.; Lv, X.; Liu, Y.; Li, J.; Du, G.; Chen, J.; Rodrigo, L.; Liu, L. Synthetic redesign of central carbon and redox metabolism for high yield production of N-acetylglucosamine in *Bacillus subtilis*. *Metab. Eng.* **2019**, *51*, 59−69.
(38) Batianis, C.; van Rosmalen, R. P.; Major, M.; van Ee, C.; Kasiotakis, A.; Weusthuis, R. A.; Martins Dos Santos, V. A. P. A tunable metabolic valve for precise growth control and increased product formation in *Pseudomonas putida*. *Metab. Eng.* **2023**, *75*, 47−57.
(39) Venayak, N.; Anesiadis, N.; Cluett, W. R.; Mahadevan, R. Engineering metabolism through dynamic control. *Curr. Opin. Biotechnol.* **2015**, *34*, 142−152.
(40) Castaño-Cerezo, S.; Pastor, J. M.; Renilla, S.; Bernal, V.; Iborra, J. L.; Cánovas, M. An insight into the role of phosphotransacetylase (*pta*) and the acetate/acetyl-CoA node in *Escherichia coli*. *Microb. Cell. Fact.* **2009**, *8*, 54.
(41) Noh, M. H.; Cha, S.; Kim, M.; Jung, G. Y. Recent advances in microbial cell growth regulation strategies for metabolic engineering. *Biotechnol. Bioprocess Eng.* **2020**, *25* (6), 810−828.
(42) Schink, S. J.; Christodoulou, D.; Mukherjee, A.; Athaide, E.; Brunner, V.; Fuhrer, T.; Bradshaw, G. A.; Sauer, U.; Basan, M.

Glycolysis/gluconeogenesis specialization in microbes is driven by biochemical constraints of flux sensing. *Mol. Syst. Biol.* **2022**, *18* (1), No. e10704.
(43) Wang, Y.; Sun, W.; Zheng, S.; Zhang, Y.; Bao, Y. Genetic engineering of *Bacillus* sp. and fermentation process optimizing for diacetyl production. *J. Biotechnol.* **2019**, *301*, 2−10.
(44) Mu, L.; Wen, J. Engineered *Bacillus subtilis* 168 produces L-malate by heterologous biosynthesis pathway construction and lactate dehydrogenase deletion. *World J. Microbiol. Biotechnol.* **2013**, *29* (1), 33−41.
(45) Renna, M. C.; Najimudin, N.; Winik, L. R.; Zahler, S. A. Regulation of the *Bacillus subtilis alsS*, *alsD*, and *alsR* genes involved in post-exponential-phase production of acetoin. *J. Bacteriol.* **1993**, *175* (12), 3863−3875.
(46) Sharma, P.; Noronha, S. Comparative assessment of factors involved in acetoin synthesis by *Bacillus subtilis* 168. *ISRN Microbiol.* **2014**, *2014*, No. 578682.
(47) Yuan, P.; Xu, M.; Mao, C.; Zheng, H.; Sun, D. Dynamically regulating glucose uptake to reduce overflow metabolism with a quorum-sensing circuit for the efficient synthesis of D-pantothenic acid in *Bacillus subtilis*. *ACS Synth. Biol.* **2023**, *12* (10), 2983−2995.
(48) Vadali, R. V.; Horton, C. E.; Rudolph, F. B.; Bennett, G. N.; San, K. Production of isoamyl acetate in *acka-pta* and/or *ldh* mutants of *Escherichia coli* with overexpression of yeast ATF2. *Appl. Microbiol. Biotechnol.* **2004**, *63* (6), 698−704.
(49) Rosero-Chasoy, G.; Rodríguez-Jasso, R. M.; Aguilar, C. N.; Buitrón, G.; Chairez, I.; Ruiz, H. A. Microbial co-culturing strategies for the production high value compounds, a reliable framework towards sustainable biorefinery implementation - an overview. *Bioresour. Technol.* **2021**, *321*, No. 124458.
(50) Arora, D.; Gupta, P.; Jaglan, S.; Roullier, C.; Grovel, O.; Bertrand, S. Expanding the chemical diversity through microorganisms co-culture: current status and outlook. *Biotechnol. Adv.* **2020**, *40*, No. 107521.
(51) Pathak, K. V.; Keharia, H.; Gupta, K.; Thakur, S. S.; Balaram, P. Lipopeptides from the banyan endophyte, *Bacillus subtilis* K1: mass spectrometric characterization of a library of fengycins. *J. Am. Soc. Mass Spectrom.* **2012**, *23* (10), 1716−1728.
(52) Li, X.; Mao, Z.; Wang, Y.; Wu, Y.; He, Y.; Long, C. ESI LC-MS and MS/MS characterization of antifungal cyclic lipopeptides produced by *Bacillus subtilis* XF-1. *J. Mol. Microbiol. Biotechnol.* **2012**, *22* (2), 83−93.
(53) Hanif, A.; Zhang, F.; Li, P.; Li, C.; Xu, Y.; Zubair, M.; Zhang, M.; Jia, D.; Zhao, X.; Liang, J.; et al. (2019) Fengycin produced by *Bacillus amyloliquefaciens* FZB42 inhibits *Fusarium graminearum* growth and mycotoxins biosynthesis. *Toxins 11* (5). DOI: DOI: 10.3390/toxins11050295.
(54) Wu, Z.; Huang, Y.; Li, Y.; Dong, J.; Liu, X.; Li, C. Biocontrol of *Rhizoctonia solani via* induction of the defense mechanism and antimicrobial compounds produced by *Bacillus subtilis* SL-44 on pepper (*Capsicum annuum* L.). *Front. Microbiol.* **2019**, *10*, 2676.
(55) Liao, J.-H.; Chen, P.; Yang, Y.; Kan, S.; Hsieh, F.; Liu, Y. Clarification of the antagonistic effect of the lipopeptides produced by *Bacillus amyloliquefaciens* BPD1 against *Pyricularia oryzae* via in situ MALDI-TOF IMS analysis. *Molecules* **2016**, *21* (12), 1670.
(56) Nifakos, K.; Tsalgatidou, P. C.; Thomloudi, E.; Skagia, A.; Kotopoulis, D.; Baira, E.; Delis, C.; Papadimitriou, K.; Markellou, E.; Venieraki, A.; et al. Genomic analysis and secondary metabolites production of the endophytic *Bacillus velezensis* Bvel1: a biocontrol agent against *Botrytis cinerea* causing bunch rot in post-harvest table grapes. *Plants* **2021**, *10* (8), 1716 DOI: 10.3390/plants10081716.
(57) Fan, H.; Ru, J.; Zhang, Y.; Wang, Q.; Li, Y. Fengycin produced by *Bacillus subtilis* 9407 plays a major role in the biocontrol of apple ring rot disease. *Microbiol. Res.* **2017**, *199*, 89−97.
(58) Li, P.; Feng, B.; Yao, Z.; Wei, B.; Zhao, Y.; Shi, S. Antifungal activity of endophytic *Bacillus* K1 against *Botrytis cinerea*. *Front. Microbiol.* **2022**, *13*, No. 935675.
(59) Xiao, J.; Guo, X.; Qiao, X.; Zhang, X.; Chen, X.; Zhang, D. Activity of fengycin and iturin A isolated from *Bacillus subtilis* z-14 on *Gaeumannomyces graminis* var. *Tritici* and soil microbial diversity. *Front. Microbiol.* **2021**, *12*, No. 682437.
(60) Zihalirwa Kulimushi, P.; Argüelles Arias, A.; Franzil, L.; Steels, S.; Ongena, M. Stimulation of fengycin-type antifungal lipopeptides in *Bacillus amyloliquefaciens* in the presence of the maize fungal pathogen *Rhizomucor variabilis*. *Front. Microbiol.* **2017**, *8*, 850.
(61) Hoste, A. C. R.; Willy, S.; Aurélien, C.; Yves, B.; Magali, D.; Mutien, G.; Philippe, J. The structure of lipopeptides impacts their antiviral activity and mode of action against SARS-CoV-2 in vitro. *Appl. Environ. Microbiol.* **2024**, *90* (11), No. e0103624.
(62) Botcazon, C.; Ramos-Martín, F.; Rodríguez-Moraga, N.; Bergia, T.; Acket, S.; Sarazin, C.; Rippa, S. Rhamnolipids and fengycins interact differently with biomimetic lipid membrane models of *Botrytis cinerea* and *Sclerotinia sclerotiorum*: lipidomics profiles and biophysical studies. *Biophys. Chem.* **2024**, *314*, No. 107305.
(63) Leconte, A.; Jacquin, J.; Duban, M.; Deweer, C.; Trapet, P.; Laruelle, F.; Farce, A.; Compère, P.; Sahmer, K.; Fiévet, V.; et al. Deciphering the mechanisms involved in reduced sensitivity to azoles and fengycin lipopeptide in *Venturia inaequalis*. *Microbiol. Res.* **2024**, *286*, No. 127816.
(64) Balleza, D.; Alessandrini, A.; Beltrán García, M. J. Role of lipid composition, physicochemical interactions, and membrane mechanics in the molecular actions of microbial cyclic lipopeptides. *J. Membr. Biol.* **2019**, *252* (2−3), 131−157.
(65) Ongena, M.; Jacques, P. *Bacillus* lipopeptides: versatile weapons for plant disease biocontrol. *Trends Microbiol.* **2008**, *16* (3), 115−125.